

Hidden Subluminous Stars among the FAUST UV sources toward OPHIUCHUS

Liliana Formiggini, Noah Brosch, Elchanan Almoznino

The Wise Observatory and the School of Physics and Astronomy

Raymond and Beverly Sackler Faculty of Exact Sciences

Tel Aviv University, Tel Aviv 69978, Israel;

lili@wise.tau.ac.il, noah@wise.tau.ac.il, nan@wise.tau.ac.il

Stuart Bowyer, Michael Lampton

Space Sciences Laboratory

University of California, Berkeley CA 94720-7450, U.S.A.;

bowyer@mofo.ssl.berkeley.edu, mlampton@ssl.berkeley.edu

Accepted 2002 MMM DD, Received 2001 MMM DD, in original form 2001 MMM DD

ABSTRACT

We present results of an analysis of a UV image in the direction of Ophiuchus, obtained with the FAUST instrument. The image contains 228 UV sources. Most of these are identified as normal early-type stars through correlations with cataloged objects. For the first time in this project we identify UV sources as such stars by selecting suitable candidates in crowded fields as the bluest objects in color-color diagrams using observations from the Wise Observatory. These candidates are then studied using low-resolution spectroscopy, which allowed the determination of spectral types to an accuracy of about one-half class, for 60 stars.

Synthetic photometry of spectral data is performed in order to predict the expected UV emission, on the basis of the photometric information. These results are used along with the Hipparcos/Tycho information, to search for sub-luminous stars. The comparison of the predicted emission with the FAUST measured magnitudes allows us to select twelve stars as highly-probable evolved hot stars. High signal-to-noise spectra are obtained for nine of these stars and Balmer line profiles were compared with the prediction of atmosphere models and with the spectrum of real stellar atmospheres. Among the nine candidates, six are classified as previously unrecognized sdB stars and two as white dwarfs. Our result indicates that indeed more bright subluminous stars are still unrecognized in the existing samples.

Key words:

Ultraviolet: stars–Galaxy: stellar content–Stars:white dwarfs–subdwarfs– Individual: Ophiuchus.

1 INTRODUCTION

In the vacuum ultraviolet range observations are very scarce and are limited to very bright sources, such as those measured by the TD-1 mission (Thompson et al. 1978). The FAUST experiment (Bowyer et al. 1993) represents a successful attempt to produce a catalog of fainter UV sources in a few regions of the sky. During the FAUST mission, about 5% of the celestial sphere was observed. First results were published in the FAUST source catalog (FSC: Bowyer et al. 1995).

One of the fields observed during the FAUST mission on

board the ATLAS-1 Shuttle mission (Lampton et al. 1993) is located in the outer region of the Ophiuchus molecular cloud. Among the fields observed by FAUST, this is the UV field nearest the galactic equator.

The Ophiuchus molecular cloud region subtends several tens of square degrees on the sky, at a distance of 125 pc. The region observed most intensively within this complex is the ρ Ophiuchus core, which is a star formation region. In addition to the core, there are diffuse and filamentary dust structures, as seen on the Palomar Sky Survey (PSS) plates. Owing to the location near the galactic center direction (l

~ 355 and $b \sim 15$), with a large number of projected stars, this is a very crowded region.

This paper presents a list of the sources detected in this field and their optical identification, obtained by correlations with published catalogues (section 2 and 3) and by photometric and spectroscopic observations performed at the Wise Observatory (section 4). The results are used below, along with Hipparcos/Tycho results, to identify new hot, sub-luminous stars (section 5). Synthetic photometry using spectral data in the ultraviolet domain allows us to predict the expected UV brightness of a source. Comparing this to the detected UV brightness yields a list of ten objects much brighter in the UV than expected. Nine of these candidates were followed up with spectroscopy to study the Balmer line profiles. We propose that six of these are hot subdwarfs and two are possibly white dwarfs, which were previously misidentified as normal main-sequence stars.

2 FAUST OBSERVATIONS OF OPHIUCHUS

FAUST (FAr Ultraviolet Space Telescope) is a wide-field ($\sim 8^\circ$ field of view) telescope with a bandpass from 1400 Å to 1800 Å and an angular resolution of 3.5 arc minutes, designed for imaging in the far ultraviolet. The FAUST telescope operated on board of the space shuttle Atlantis during the ATLAS-1 mission and imaged 22 sky fields. Details of the image reconstruction and performance are given in Bowyer et al. (1993). A catalog of the 4698 UV sources detected by FAUST and of their optical identification, based on positional coincidence with entries from catalogues of stars and galaxies, was produced by Bowyer et al. (1995). Most of the 22 fields were analyzed at the Tel Aviv University and accurate identifications were obtained with the help of ground-based spectroscopy. The results of this systematic analysis have already been presented for the following sky regions: the North Galactic Pole (Brosch et al. 1995); the Virgo cluster region (Brosch et al. 1997); the Coma Cluster region (Brosch et al. 1998); the Fourth Galactic Quadrant region (Brosch et al. 2000a); a region near the North Galactic Pole (Brosch et al. 2000b) and the Antennae and NGC 6752 regions (Daniels et al. 2001). One of the fields observed by FAUST is centered at $\alpha_{1950} = 17^h 20^m$, $\delta_{1950} = -20^\circ 00'$, on the outskirts of the Ophiuchus cloud, $14^\circ.3$ NE from the center of the molecular cloud, in a very crowded, low galactic latitude region.

The total sky area covered by the FAUST Ophiuchus image is ~ 49.4 square degrees (\square°). We analyzed this image using an impartial source detector algorithm (Brosch et al. 1995), that was adopted for the FAUST fields already analyzed at Tel-Aviv. This algorithm takes into account the different image depths that affect various regions of the image and is characterized by a signal-to-noise threshold (Brosch et al. 1997). This impartial automatic algorithm detected 228 UV sources in the Ophiuchus FAUST frame. The FAUST image is shown in Fig 1.

Table 1 lists the coordinates of the detected sources with their calculated coordinates and their UV magnitude. The UV monochromatic magnitude is defined as

$$m_{UV} = -21.175 - 2.5 * \log(FD) \quad (1)$$

where the flux density FD is in $\text{erg}/\text{sec}/\text{cm}^2/\text{\AA}$. The flux

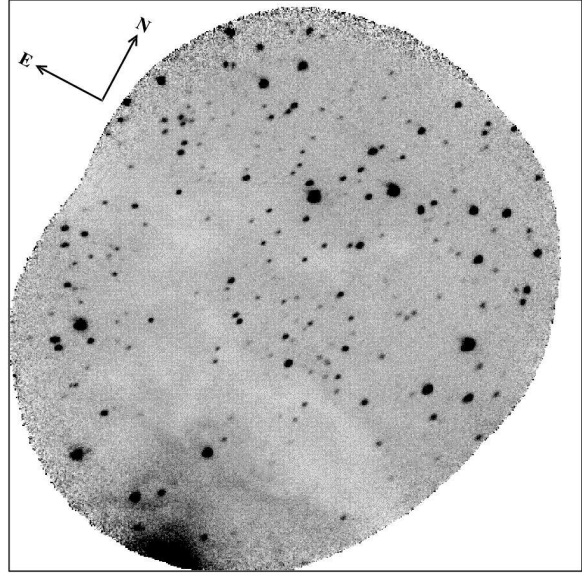


Figure 1. The FAUST image of the Ophiuchus field. The elongated stellar images are the results of imperfect alignment of the time-tagged positions. Note the lightly colored patches near the center and in the Southern part of the image; these are dust clouds blocking part of the background.

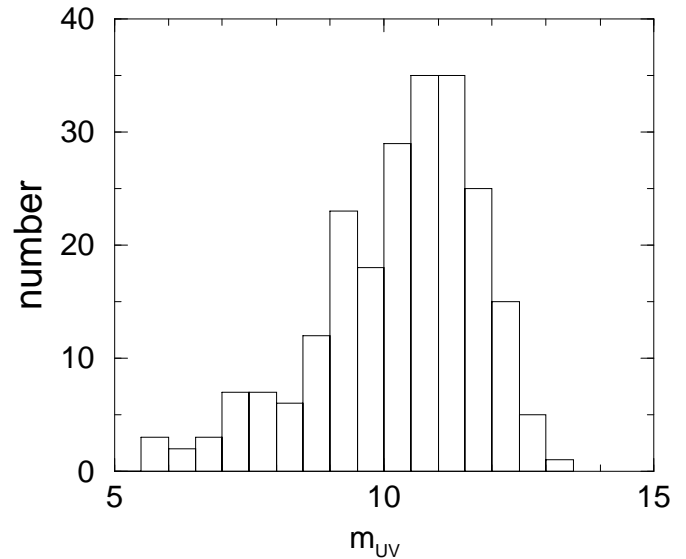


Figure 2. Histogram of the number of sources versus the measured Faust magnitudes.

density was derived from the count rate of FAUST, as explained in Brosch et al. (1995). The error in the flux takes into account both the instrumental error and the systematic one resulting from the laboratory calibration of FAUST, as explained in Brosch et al. (1997). Fig 2 shows the distribution in UV flux of the detected sources expressed as monochromatic magnitudes. As previously mentioned, FAUST sources in this field have already been extracted by Bowyer et al. (1995)-FSC using a flux-limited algorithm. We compared our detections with that from FSC and found that all but nine sources have already been listed in the

FSC. Although the detection methods are different, we believe that these additional sources are true detections. The last column of Table 1 lists the number of the source in the FSC catalog. An asterisk marks the nine new detections.

3 IDENTIFICATIONS OF THE FAUST SOURCES

The first approach to the identification work has been the search for positional coincidence with various catalogues such as the Smithsonian Astrophysical Observatory (SAO 1966) and the Hipparcos Input Catalog (Turon *et al.* 1993), mainly through the SIMBAD data base. In addition to the positional coincidence ($3' \times 3'$ error box), some astrophysical constraints have been applied, such as that when more than one counterpart lies in the error box of a UV source, the bluest or brightest or earlier-type star was accepted. This search led to a positive identification of 166 sources ($\simeq 73\%$).

For the remaining sources no plausible counterpart could be found using correlations with catalogues entries. This sky region is very crowded, owing to the low galactic latitude of the FAUST frame, and a visual inspection of the E and O prints of the Palomar Sky Survey (PSS) does not allow one to select a reasonable number of candidates among the many stars inside the error box of the UV source.

The adopted approach was to first narrow down the list of possible objects by obtaining multicolor broad-band photometry of the region around each of the unidentified UV sources. The color-color diagram for all the stars inside the error box was used to select the bluest objects, and low-resolution spectra were obtained for these in order to assign a most probable counterpart to the FAUST source.

4 GROUND-BASED OBSERVATIONS

The search for an optical counterpart to the unidentified FAUST UV sources was performed with ground-based photometry and spectroscopy obtained at the Wise Observatory.

4.1 Multicolor photometry

For each of the 62 unidentified FAUST sources, three CCD short exposures have been obtained in blue, visual and red (B, V, R) at the 1m telescope of the Wise Observatory. The camera used is a Tektronix thinned and back-illuminated 1024×1024 pixel CCD, which images a field of view of $12'$.

Typical exposure times were 180 sec for B, 90 sec for V, and 80 sec for R. Photometric reduction was performed using the DAOPHOT package, and the instrumental magnitudes and color indices $(b-v)$ and $(v-r)$ were obtained for all the stars inside a $3' \times 3'$ error box around each UV source.

The mean intrinsic colors of a star of a given spectral type and luminosity class are well-defined (Johnson 1966). This implies that a color-color diagram can be used to select stars of different spectral types. By plotting the instrumental color indices for all the objects within the error box, the bluest (or earliest-type) stars should reside in a well-defined part of the diagram.

However, the mean colors are well-determined only for

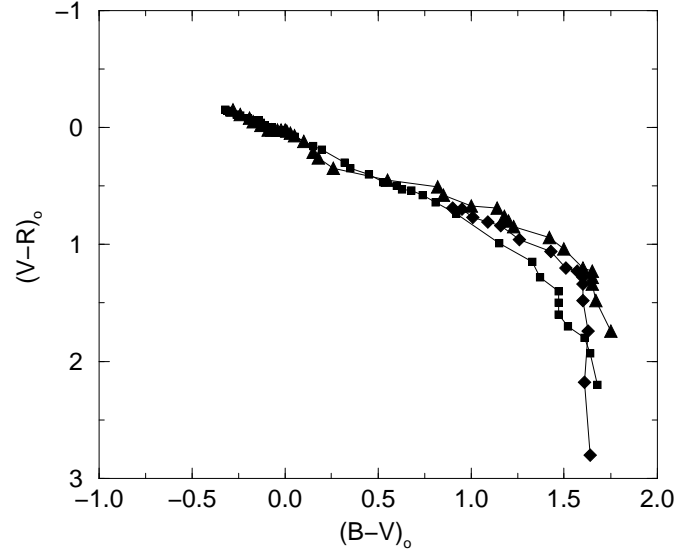


Figure 3. $(V-R)_0$ versus $(B-V)_0$ colors diagram for stars. Main sequence stars are plotted as squares, giant stars as diamonds and supergiants are plotted as triangles.

unreddened stars. Hence we must address the question on how reddening may affect the measured colors and if the use of reddened colors could bias our selection procedure, which is based on the $(b-v)$ and $(v-r)$ colors. In the following, we assume that there are no significant color terms in the transformation from instrumental to standard colors. This is justified by numerous absolute-photometry studies performed at the Wise Observatory with CCD cameras.

We plot in Fig 3 the mean colors $(B-V)_0$ versus $(V-R)_0$ for main-sequence, giant and supergiant stars (Johnson 1966). Note that the intrinsic $(B-V)_0$ of a B0 type main sequence star is -0.30 while it is $(B-V)_0 = +0.82$ for a K0 star. It can be seen that, up to $(B-V)_0 \simeq 1.0$, the locus of the intrinsic colors of the stars is well-defined as a linear relation with an approximate slope of 0.80 for all the luminosity classes. The lines representing the supergiant and bright giant stars diverge from the main sequence line only for the very red stars with $(B-V) > 1.0$. From the average extinction curve (Savage & Mathis 1979), the slope of the reddening line $E(V-R)/E(B-V)$ is 0.78, very similar to the slope of the intrinsic color-color relation. Hence, the use of instrumental colors instead of intrinsic ones will only underestimate the spectral type along the reddening line. This increases our confidence that the use of the two-color diagram $(v-r)$ versus $(b-v)$ is a suitable tool for selecting the blue color-excess objects inside the error box of the FAUST source.

Fig 4 shows the PSS image of the field around the UV source N.92, whose location is marked by a cross. The brightest star in the field is HD 156169, classified as K0 III.

Three short CCD exposures in B, V, and R were obtained for this field and blue, visual and red instrumental magnitudes were measured for all the objects in a $3' \times 3'$ box centered on the cross. The $(b-v)$ versus $(v-r)$ diagram is shown in Fig 5. It can be seen that all the measured objects, including the one marked by an asterisk, lie on a well defined range of color indices. This object, characterized by the bluest instrumental $(b-v)$ color, was picked up as the

Table 1. Detected FAUST sources in the Ophiuchus field

Id.no.	α_{2000}	δ_{2000}	m_{UV}	FAUST no.
1	17 34 52.46	-16 38 47.44	7.66± 0.20	4219
2	17 30 02.86	-16 03 02.95	8.86± 0.20	4174
3	17 31 05.91	-16 11 30.41	11.03± 0.44	4183
4	17 29 06.64	-16 02 38.11	10.92± 0.36	4167
5	17 32 37.55	-16 39 07.30	9.01± 0.20	4196
6	17 29 24.29	-16 36 25.46	7.42± 0.17	4169
7	17 34 12.77	-17 09 18.44	9.15± 0.20	4211
8	17 33 44.52	-17 07 13.78	9.58± 0.21	4204
9	17 23 45.05	-16 03 46.08	10.90± 0.29	4127
10	17 31 17.31	-17 09 23.53	7.06± 0.17	4184
11	17 37 44.70	-17 51 27.32	7.58± 0.19	4242
12	17 25 38.48	-16 28 00.63	11.89± 0.47	4142
13	17 25 38.87	-16 36 50.61	11.57± 0.42	4143
14	17 35 41.52	-17 50 09.55	11.07± 0.36	4227
15	17 23 23.91	-16 29 18.81	11.02± 0.31	4126
16	17 18 38.14	-16 01 25.40	8.80± 0.19	4077
17	17 39 18.40	-18 25 47.55	8.52± 0.23	4250
18	17 34 04.30	-17 51 11.68	11.54± 0.34	4206
19	17 28 42.29	-17 15 39.92	8.63± 0.17	4162
20	17 30 33.18	-17 29 36.13	11.24± 0.35	4179
21	17 35 15.05	-18 03 16.67	10.86± 0.31	4221
22	17 26 52.57	-17 06 55.83	10.85± 0.28	4155
23	17 34 49.35	-18 05 42.44	10.99± 0.26	4218
24	17 32 18.21	-17 48 53.36	12.28± 0.49	4193
25	17 28 54.02	-17 23 36.28	9.17± 0.18	4164
26	17 29 47.23	-17 36 13.25	9.86± 0.20	4171
27	17 35 22.87	-18 15 56.02	9.17± 0.18	4224
28	17 25 28.88	-17 05 59.25	11.44± 0.35	4140
29	17 36 20.24	-18 25 13.77	9.79± 0.22	4233
30	17 39 06.33	-18 44 00.14	9.34± 0.22	4249
31	17 33 23.46	-18 03 09.05	12.10± 0.50	4200
32	17 34 40.00	-18 14 22.22	9.96± 0.21	4215
33	17 21 08.67	-16 38 48.83	10.79± 0.27	4103
34	17 16 14.01	-16 04 26.31	9.74± 0.21	4057
35	17 35 06.68	-18 19 40.59	9.14± 0.18	4220
36	17 32 13.03	-18 02 37.64	12.05± 0.47	4191
37	17 20 03.40	-16 40 51.02	8.35± 0.17	4092
38	17 19 35.72	-16 32 49.49	11.68± 0.41	*
39	17 35 57.63	-18 35 07.11	10.08± 0.22	4228
40	17 14 28.13	-15 57 01.76	9.67± 0.20	4042
41	17 16 08.68	-16 14 02.60	9.57± 0.22	4056
42	17 30 10.18	-17 56 16.81	11.31± 0.28	4175
43	17 39 32.25	-19 01 26.78	10.32± 0.33	4252
44	17 33 30.15	-18 20 21.28	12.03± 0.43	4201
45	17 26 33.76	-17 36 09.30	11.53± 0.32	4149
46	17 32 23.70	-18 14 41.78	12.63± 0.69	*
47	17 34 24.73	-18 37 05.44	9.64± 0.19	4214
48	17 18 14.01	-16 40 22.15	10.87± 0.28	4071
49	17 33 25.99	-18 31 32.59	11.04± 0.26	4202
50	17 38 27.88	-19 05 14.45	10.99± 0.34	4245
51	17 22 03.21	-17 13 59.85	9.00± 0.18	4111
52	17 15 35.01	-16 26 17.91	10.56± 0.29	4051
53	17 22 24.52	-17 20 46.12	7.57± 0.17	4114
54	17 29 46.64	-18 08 30.52	11.94± 0.37	4172
55	17 34 20.36	-18 47 01.07	9.03± 0.18	4212
56	17 28 14.08	-18 00 41.09	13.13± 0.74	4161
57	17 26 46.17	-17 53 13.72	10.64± 0.23	4153
58	17 20 24.82	-17 12 56.01	10.24± 0.22	4094
59	17 20 53.96	-17 19 10.32	11.47± 0.34	*

Id no.	α_{2000}	δ_{2000}	m_{UV}	FAUST no.
60	17 26 32.59	-18 05 38.41	10.50± 0.23	4150
61	17 37 02.98	-19 21 17.12	10.70± 0.27	4237
62	17 32 33.13	-18 50 57.63	12.62± 0.71	4195
63	17 22 35.72	-17 42 18.03	9.56± 0.19	4118
64	17 12 52.33	-16 29 27.72	11.69± 0.49	4036
65	17 29 43.35	-18 33 53.18	10.32± 0.21	4273
66	17 26 42.46	-18 15 53.31	10.56± 0.22	4151
67	17 31 36.29	-18 51 01.23	13.75± 1.16	4188
68	17 29 26.98	-18 40 30.56	8.73± 0.17	4168
69	17 23 25.09	-17 58 09.90	9.64± 0.20	4125
70	17 11 26.94	-16 28 30.50	9.44± 0.22	4027
71	17 25 19.95	-18 16 56.65	8.35± 0.17	4138
72	17 32 21.36	-19 03 37.49	11.61± 0.34	4192
73	17 22 19.42	-17 53 10.31	12.18± 0.54	4113
74	17 28 08.31	-18 36 38.64	15.55± 6.75	4160
75	17 19 54.48	-17 46 14.21	5.64± 0.16	4088
76	17 33 15.22	-19 22 48.21	9.68± 0.20	4199
77	17 16 08.51	-17 18 32.16	10.74± 0.27	4055
78	17 21 15.58	-18 02 45.70	9.08± 0.18	4104
79	17 24 37.01	-18 27 32.35	5.63± 0.16	4133
80	17 22 50.54	-18 11 32.59	12.02± 0.46	4120
81	17 37 35.10	-20 03 59.62	10.47± 0.23	4240
82	17 17 02.15	-17 38 52.84	9.42± 0.18	4063
83	17 35 36.04	-19 54 08.54	9.42± 0.18	4225
84	17 23 27.53	-18 26 10.14	11.14± 0.32	4124
85	17 17 35.65	-17 50 52.15	7.76± 0.18	4066
86	17 14 19.60	-17 27 02.94	7.21± 0.17	4040
87	17 12 12.28	-17 13 37.90	7.48± 0.18	4030
88	17 27 01.10	-18 59 20.70	10.45± 0.21	4156
89	17 38 35.48	-20 19 01.36	11.59± 0.42	4246
90	17 24 26.69	-18 50 18.71	9.22± 0.18	4130
91	17 30 37.91	-19 33 34.58	10.77± 0.26	4178
92	17 16 48.29	-17 55 45.54	11.54± 0.41	4061
93	17 27 49.01	-19 16 47.86	11.30± 0.31	4159
94	17 39 21.47	-20 44 02.54	8.92± 0.16	4251
95	17 34 24.41	-20 06 24.04	11.04± 0.26	4213
96	17 15 31.49	-17 50 31.23	11.68± 0.43	4049
97	17 19 43.43	-18 21 47.62	12.04± 0.59	4086
98	17 10 17.38	-17 19 08.68	9.97± 0.23	4021
99	17 12 27.86	-17 35 08.11	10.71± 0.27	4032
100	17 25 45.63	-19 14 27.95	10.78± 0.25	4144
101	17 37 55.40	-20 40 58.58	9.01± 0.18	4243
102	17 19 13.73	-18 31 06.46	11.76± 0.46	4082
103	17 35 50.46	-20 29 43.22	11.96± 0.49	4229
104	17 15 42.83	-18 10 22.73	11.32± 0.34	4052
105	17 20 15.65	-18 49 24.94	8.07± 0.18	4093
106	17 26 21.82	-19 30 34.55	10.34± 0.21	4147
107	17 38 51.22	-20 58 58.05	9.22± 0.20	4247
108	17 20 52.91	-18 54 05.27	9.67± 0.19	4100
109	17 22 28.75	-19 05 54.60	10.12± 0.23	4115
110	17 35 26.35	-20 39 48.98	10.30± 0.23	4223
111	17 14 27.28	-18 11 25.52	11.47± 0.33	4041
112	17 09 02.26	-17 34 15.83	8.03± 0.19	4014
113	17 34 14.75	-20 33 28.26	11.79± 0.43	4209
114	17 13 53.10	-18 12 12.66	10.80± 0.25	4039
115	17 36 51.12	-20 57 45.45	11.21± 0.31	4236
116	17 35 41.66	-20 49 42.58	11.42± 0.29	4226
117	17 15 25.96	-18 23 44.05	12.02± 0.48	*
118	17 12 27.46	-18 07 32.86	7.69± 0.18	4033

Id.no.	α_{2000}	δ_{2000}	m_{UV}	FAUSTno.
119	17 15 00.35	-18 24 12.47	12.50± 0.66	4045
120	17 23 15.15	-19 26 48.78	10.40± 0.23	4123
121	17 40 17.67	-21 21 51.19	12.88± 1.51	*
122	17 25 26.73	-19 43 55.33	10.71± 0.23	4139
123	17 37 40.33	-21 11 24.90	10.20± 0.22	4241
124	17 26 45.91	-19 58 41.64	12.61± 0.55	4152
125	17 11 04.39	-18 09 26.68	10.80± 0.27	4024
126	17 34 46.89	-21 03 16.45	10.24± 0.23	4216
127	17 27 11.82	-20 18 10.39	8.86± 0.17	4157
128	17 24 33.17	-19 56 18.99	11.84± 0.45	4131
129	17 17 31.16	-19 08 33.83	11.35± 0.31	4065
130	17 12 40.39	-18 32 32.76	11.63± 0.36	4035
131	17 11 57.93	-18 27 37.48	11.47± 0.37	4028
132	17 37 27.37	-21 33 19.55	9.02± 0.19	4238
133	17 08 29.88	-18 11 35.95	7.85± 0.18	4011
134	17 36 56.88	-21 33 13.16	9.50± 0.19	4235
135	17 36 24.99	-21 29 07.67	10.86± 0.27	4232
136	17 27 12.83	-20 27 02.22	10.32± 0.22	4158
137	17 09 08.91	-18 16 33.79	10.19± 0.25	4011
138	17 29 01.18	-20 44 16.02	12.13± 0.40	4166
139	17 19 55.06	-19 41 45.15	9.46± 0.19	4089
140	17 13 41.60	-18 58 09.32	11.01± 0.28	4038
141	17 25 00.72	-20 21 26.23	11.25± 0.27	4135
142	17 22 32.10	-20 03 47.70	11.05± 0.29	4116
143	17 16 25.51	-19 19 06.63	12.10± 0.38	4058
144	17 08 21.83	-18 24 01.73	9.19± 0.19	4009
145	17 23 14.53	-20 13 19.36	10.75± 0.23	4122
146	17 36 06.38	-21 42 43.63	11.29± 0.36	4230
147	17 10 42.29	-18 45 34.57	9.93± 0.21	4023
148	17 20 49.18	-20 01 34.49	11.36± 0.30	4098
149	17 14 43.31	-19 24 38.14	10.24± 0.21	4043
150	17 32 51.56	-21 33 35.12	11.49± 0.35	4197
151	17 25 49.21	-20 46 24.36	9.15± 0.18	4145
152	17 15 35.36	-19 32 12.73	10.64± 0.25	4050
153	17 37 35.13	-22 05 34.82	11.15± 0.38	4239
154	17 35 24.89	-22 03 20.65	6.09± 0.16	4222
155	17 18 28.74	-19 57 33.35	10.18± 0.20	4073
156	17 14 59.37	-19 31 47.80	10.30± 0.22	4046
157	17 25 23.64	-20 50 27.30	9.06± 0.18	4137
158	17 31 03.17	-21 28 15.35	9.75± 0.19	4181
159	17 21 48.13	-20 24 22.27	12.19± 0.44	4108
160	17 33 10.00	-21 44 42.80	11.19± 0.29	4198
161	17 20 51.98	-20 20 29.30	10.24± 0.21	4099
162	17 21 01.55	-20 26 46.62	10.58± 0.22	4102
163	17 17 53.39	-20 09 38.39	11.77± 0.37	4068
164	17 22 00.19	-20 43 14.02	9.51± 0.18	4109
165	17 36 34.05	-22 26 57.86	7.32± 0.18	4234
166	17 10 16.94	-19 26 45.91	5.65± 0.16	4020
167	17 38 11.86	-22 35 49.08	11.06± 0.40	4224
168	17 34 15.16	-22 12 58.31	8.80± 0.18	4210
169	17 21 26.92	-20 43 49.41	10.33± 0.22	4105
170	17 32 31.95	-22 01 55.86	11.54± 0.34	4194
171	17 24 06.80	-21 05 01.94	11.00± 0.29	4128
172	17 18 49.88	-20 29 59.76	11.66± 0.34	4079
173	17 36 05.96	-22 32 38.50	7.30± 0.18	4231
174	17 31 37.40	-22 02 11.91	10.63± 0.25	4187
175	17 17 51.09	-20 26 54.97	9.16± 0.18	4067
176	17 25 55.64	-21 24 19.83	10.75± 0.25	4146
177	17 15 18.48	-20 17 00.77	10.31± 0.22	4047
178	17 22 21.23	-21 06 47.73	11.25± 0.30	4112
179	17 19 11.62	-20 46 00.91	10.63± 0.22	4081
180	17 25 40.30	-21 36 33.04	10.48± 0.24	4141
181	17 20 56.90	-21 05 24.68	7.83± 0.18	4101

Id. no.	α_{2000}	δ_{2000}	m_{UV}	FAUST no.
182	17 18 32.02	-20 47 23.15	10.49± 0.24	4074
183	17 08 54.26	-19 40 14.29	10.01± 0.21	4013
184	17 33 37.03	-22 37 43.09	11.33± 0.34	4203
185	17 19 17.46	-21 03 02.31	11.08± 0.34	4083
186	17 17 23.82	-20 54 48.14	10.01± 0.21	4064
187	17 21 59.79	-21 24 45.48	12.35± 0.47	4110
188	17 18 12.70	-21 00 14.94	10.68± 0.27	4069
189	17 20 42.84	-21 17 32.00	12.96± 1.15	4097
190	17 11 21.78	-20 24 27.24	6.92± 0.17	4025
191	17 33 53.67	-22 58 49.90	10.00± 0.22	4205
192	17 17 00.99	-21 08 15.18	10.44± 0.26	4062
193	17 06 56.00	-19 56 57.68	10.08± 0.25	4007
194	17 12 11.13	-20 36 02.94	11.16± 0.29	4029
195	17 08 32.94	-20 12 54.43	8.01± 0.18	4012
196	17 34 13.41	-23 13 25.58	11.21± 0.36	4208
197	17 14 53.61	-21 04 56.38	9.33± 0.19	4044
198	17 09 45.60	-20 23 09.08	12.08± 0.55	4017
199	17 18 36.17	-21 34 28.09	10.56± 0.23	4075
200	17 30 37.20	-23 02 51.40	10.95± 0.29	4177
201	17 31 06.05	-23 10 38.63	8.83± 0.18	4182
202	17 10 05.87	-20 45 57.25	9.45± 0.19	4019
203	17 22 53.11	-22 20 13.20	10.89± 0.32	4119
204	17 28 45.44	-22 56 16.96	11.64± 0.40	4163
205	17 19 48.48	-21 56 20.03	11.76± 0.37	4085
206	17 18 43.12	-21 52 17.61	10.93± 0.25	4076
207	17 23 52.66	-22 36 25.83	11.13± 0.42	*
208	17 06 35.29	-20 42 32.99	9.78± 0.21	4006
209	17 22 35.07	-22 41 22.11	10.51± 0.24	4117
210	17 12 38.07	-21 34 16.36	10.13± 0.25	4034
211	17 18 16.43	-22 13 47.84	11.70± 0.39	4070
212	17 23 12.47	-23 00 26.34	6.84± 0.18	4121
213	17 31 03.06	-23 52 35.98	8.82± 0.19	4180
214	17 08 29.17	-21 19 56.64	10.98± 0.29	4110
215	17 18 46.62	-22 41 00.90	11.65± 0.45	4078
216	17 11 23.52	-21 52 22.69	11.82± 0.50	4026
217	17 10 43.65	-21 59 00.33	11.23± 0.33	4022
218	17 18 24.85	-22 55 54.87	11.81± 0.52	4072
219	17 24 26.09	-23 41 52.78	10.99± 0.36	4129
220	17 15 11.33	-22 40 21.19	12.33± 0.58	*
221	17 24 52.83	-23 56 02.37	8.19± 0.22	4134
222	17 26 26.06	-24 11 06.47	6.89± 0.19	4148
223	17 09 07.14	-22 13 19.09	11.33± 0.46	*
224	17 12 24.53	-22 55 30.89	10.03± 0.27	4031
225	17 25 14.24	-24 37 08.66	7.39± 0.20	4136
226	17 18 55.17	-23 59 44.35	11.16± 0.49	4080
227	17 20 40.36	-24 16 08.22	8.98± 0.23	4096
228	17 23 57.81	-24 51 04.17	6.31± 0.18	*

possible counterpart to the UV source to be observed spectroscopically. This star, marked by an arrow in Fig 4, was observed later at the Wise Observatory and classified as an early-A type of the proper apparent V magnitude to have the measured UV flux. This test demonstrates the validity of selecting counterparts of UV sources based on color-color diagrams.

For all the UV sources (but one) for which we applied the photometric method, the two-color diagram allowed the selection of one or a few candidates with a blue color excess.

The magnitudes and colors used for the selection are instrumental. Our color calibration is poor, since photometric standard stars were obtained only on a few of the observation nights. We compared the Wise calibrated magnitudes with the m_v magnitude from the Guide Star Catalog (Lasker

et al. 1987) and found a systematic difference of 0.1 mag for our visual magnitude; this is quite acceptable and does not affect the selection criteria.

Fig. 6 shows the calibrated V–R versus B–V for the stars measured at Wise. The colors for main sequence stars of known spectral type (Johnson 1966) are also marked. It is evident that if we correct for the systematic shift in our magnitudes, and apply the 0.1 mag shift to the visual magnitude, the measured points will lie on the the photoelectric relation.

4.2 Spectroscopy

The next step was to obtain spectra of the color-excess candidates, selected by the multicolor photometry. We used the

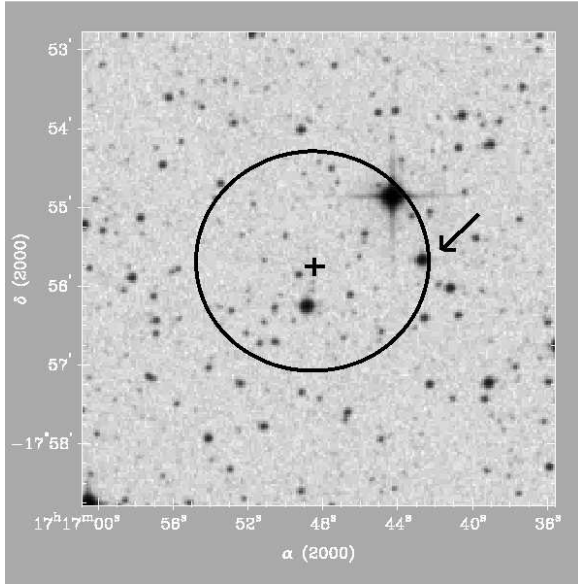


Figure 4. PSS segment of the field around UV source N. 92. The position of the FAUST source is marked by a cross, and the optical counterpart by an arrow. The circle indicates the site of the positional error expected for this Faust source.

FOSC (Faint Object Spectrometer Camera) at the $f/7$ focal position of the 1.0-meter telescope at the Wise Observatory and the Tektronix 1024x1024 pixel CCD. The wavelength coverage used was from $\sim 4000\text{\AA}$ to $\sim 8000\text{\AA}$ with a resolution of $\sim 4\text{\AA}$ per pixel. All images were bias-subtracted and flat-fielded, and all spectra were extracted and wavelength and flux-calibrated using IRAF.

Spectral types were derived by comparing the observed spectra with those in the spectral atlases of Jacoby et al. (1984) and of Silva & Cornell (1992). Spectral subclass types could not be assigned, since the spectral coverage did not include the blue region from $\sim 3800\text{\AA}$ to $\sim 4000\text{\AA}$ where the relevant lines are located. Only a broad subclass is defined here, such as early or late, and is marked in Table 2 with the symbols e or l. Most spectra show only prominent Balmer absorption lines and are classified as early-type stars, from mid-B to late-A or F.

The low resolution of the spectra prevents a luminosity classification, but supergiants appear in most cases to be ruled out, because supergiant B stars have almost no $H\alpha$ absorption while late-A supergiants show reasonably deep He I $\lambda 5876\text{\AA}$ absorption.

Table 2 lists the optical counterparts to the FAUST sources and their spectral types obtained from SIMBAD or derived from our observations. The spectroscopic observations obtained at Wise allowed us to assign a spectral type to 60 stars among the 62 unidentified sources.

5 RESULTS

The most evident result is that all the UV sources but one have been positively associated with a star of known or observed spectral type. This very high percentage of identifications is the result of our extensive observational program.

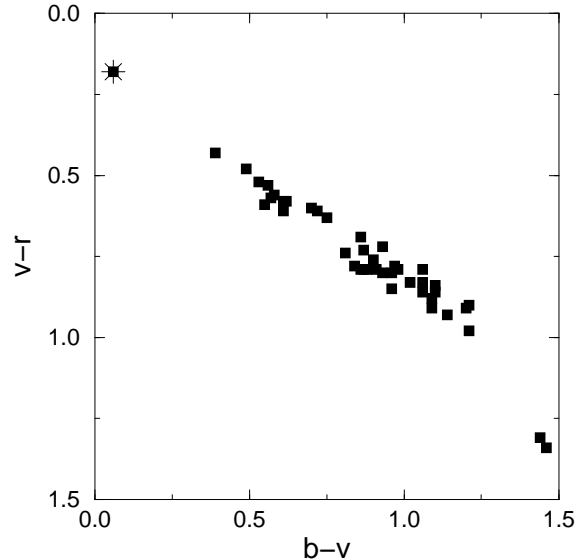


Figure 5. The two color diagram ($v-r$) versus ($b-v$) for the stars measured in a three arcmin box around the N. 92 source. The asterisk marks the star chosen as candidate, further classified as an early-A star.

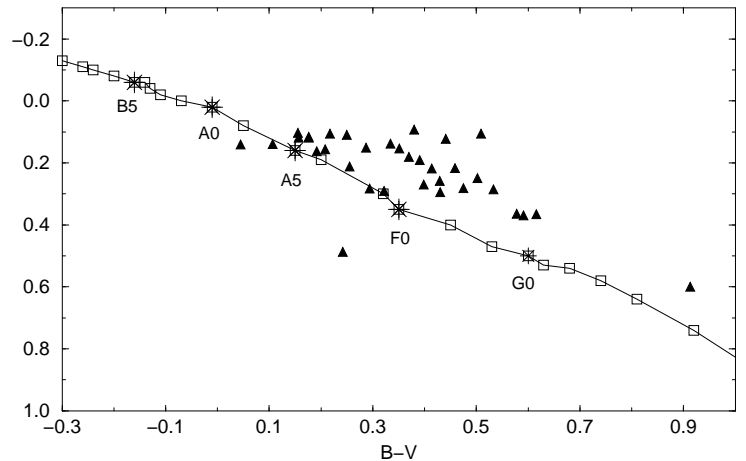


Figure 6. The ($V-R$) versus ($B-V$) diagram for the photometrically observed stars. Triangles represent the stars for which photometric calibration was available. Squares indicates the main sequence stars (Johnson et al. 1966).

For one source, N.207, no suitable candidate could be selected from the photometry. For N.97, the bluest candidate selected by the photometry was too faint to be observed with the FOSC camera. A globular cluster (M9) is identified as the optical counterpart of source N.102.

Table 3 lists the distribution of the identified sources according to spectral type. It is clear that almost all the stars belong to the B or A spectral types. No star later than G was found. Only two sources, N.96 and N.152, are identified with an early G-type star. The $[UV-v]$ color for both these

Table 2. Identified FAUST sources

Id no.	α_{2000}	δ_{2000}	Proposed id.	Sp. Type	m_b	m_v
1	17 34 46.98	-16 37 25.9	SAO 160650	B9II/III	8.76	8.74
2	17 29 53.77	-16 00 57.5	SAO 160582	A0IV	8.62	8.48
3	17 30 57.66	-16 09 53.6	SAO 160605	A2/A3IV	9.77	9.42
4	17 28 55.86	-16 01 10.1	SAO 160569	A0V	10.13	9.95
5	17 32 32.40	-16 38 34.4	HD 158924	B9II/III	9.54	9.40
6	17 29 18.35	-16 35 26.7	SAO 160574	B8Vne	8.92	8.894
7	17 34 05.76	-17 08 18.2	SAO 160644	B9II	9.96	9.83
8	17 33 37.64	-17 06 34.3	HD 159123	B9IV	10.43	10.13
9	17 23 53.00	-16 02 11.0	wise(172353-160211)	A(e)	11.2	
10	17 31 12.83	-17 08 31.7	SAO 160608	B0II	8.32	8.20
11	17 37 39.10	-17 49 76.1	SAO 160702	B1Ib	8.58	8.56
12	17 25 35.48	-16 26 48.1	SAO 160536	A3III	9.9	9.57
13	17 25 33.00	-16 35 40.0	wise(172533-163540)	B(I)	11.4	
14	17 35 33.00	-17 49 33.0	wise(173533-174933)	B(e)	11.2	
15	17 23 21.00	-16 28 27.0	wise(172321-162827)	A(e)	10.8	
16	17 18 39.22	-16 01 47.1	SAO 160445	A3III	7.78	7.61
17	17 39 18.01	-18 24 41.4	SAO 160720	B1/B2Ib/II	9.17	9.07
18	17 33 58.99	-17 50 10.6	SAO 160642	F2V	8.27	7.93
19	17 28 39.29	-17 14 58.2	HD 158195	B2III	10.18	10.11
20	17 30 30.00	-17 29 09.0	wise(173030-172909)	A(e)	11.2	
21	17 35 11.00	-18 02 12.0	wise(173511-180212)	B(e)	10.6	
22	17 26 49.00	-17 06 10.0	wise(172649-170610)	B(e)	11.2	11.1
23	17 34 41.00	-18 04 53.0	wise(173441-180453)	A(e)	10.5	
24	17 32 14.85	-17 46 54.8	HD 158841	A0III	11.4	11.3
25	17 28 51.28	-17 23 21.9	HD 158231	B9III	10.64	10.5
26	17 29 44.79	-17 35 34.1	SAO 160581	A1V	9.14	8.97
27	17 35 20.04	-18 14 42.9	SAO 160661	B9.5/A0V	9.33	9.17
28	17 25 26.00	-17 05 25.0	wise(172526-170525)	A(e)		11.9
29	17 36 18.40	-18 24 23.8	HD 159590	B9.5V	10.23	10.1
30	17 39 08.00	-18 43 13.8	HD 160144	B9III/IV	10.21	10.2
31	17 33 19.43	-18 02 33.5	SAO 160632	A1III/IV	9.69	9.32
32	17 34 33.39	-18 13 15.0	SAO 160649	F0IV/V	7.49	7.11
33	17 21 08.00	-16 38 38.0	wise(172108-163838)	A(e)	12.4	
34	17 16 18.42	-16 05 48.0	SAO 160414	A0V	9.32	9.06
35	17 35 01.97	-18 19 39.1	SAO 160658	A0IV	9.97	9.84
36	17 32 19.00	-18 02 39.0	wise(173210-180239)	B	10.7	
37	17 20 02.55	-16 40 55.7	SAO 160467	B9IV	8.76	8.62
38	17 19 33.00	-16 32 42.0	wise(171933-163242)	A(e)	11.2	
39	17 35 55.22	-18 34 00.4	HD 159506	A0V	9.79	9.64
40	17 14 32.89	-15 57 22.9	SAO 160395	A0	8.81	8.66
41	17 16 11.98	-16 15 25.1	SAO 160412	B9V	9.93	9.83
42	17 30 18.58	-17 56 26.7	wise(173018-175627)	no sp	10.81	10.4
	17 30 00.58	-17 55 05.7	HD 158442	A2	10.35	10.11
43	17 39 28.19	-19 01 07.3	HD 160219	B9IV	10.43	10.2
44	17 33 27.00	-18 20 23.2	SAO 160635	F3V	8.20	7.76
45	17 26 31.65	-17 35 13.5	HD 157859	A2V	10.26	9.92
46	17 32 22.00	-18 15 15.0	wise(173222-181515)	A(I)	11.1	
47	17 34 21.10	-18 36 21.7	HD 159246	B9III	9.96	9.81
48	17 18 14.25	-16 40 48.3	SAO 160436	A0IV	9.52	9.35
49	17 33 25.00	-18 31 16.0	wise(173325-183116)	A(e)	11.3	10.8
50	17 38 21.82	-19 04 26.8	HD 159976	A0IV	10.74	10.5
51	17 22 01.75	-17 13 11.1	SAO 160496	A5III	8.68	8.42
52	17 15 39.00	-16 27 54.0	wise(171539-162754)	B	12.4	
53	17 22 22.56	-17 20 25.6	SAO 160500	A0V	8.10	7.97
54	17 29 44.42	-18 07 47.1	HD 158391	A8V	10.66	10.4
55	17 34 17.64	-18 46 36.2	SAO 160647	B8II/III	9.79	9.70
56	17 28 13.00	-18 00 24.0	wise(172813-180024)	A(I)	11.2	
57	17 26 44.15	-17 52 34.6	HD 157897	A0IV/V	9.94	9.84
58	17 20 25.63	-17 13 15.0	HD 156830	B9III	10.72	10.6

Id no.	α_{2000}	δ_{2000}	Proposed id.	Sp. Type	m_b	m_v
59	17 20 52.71	-17 20 05.2	V441 OPH	A0	11.5	11.8
60	17 26 31.02	-18 05 07.4	HD 157860	B9III	10.46	10.27
61	17 37 00.00	-19 20 22.0	wise(173700-192022)	A(e)	10.6	
62	17 32 32.00	-18 50 03.0	wise(173232-185003)	A(e)	11.4	10.4
63	17 19 40.66	-17 39 23.4	SAO 160505	A1IV/V	8.35	8.22
64	17 12 58.58	-16 30 52.6	SAO 160368	A1m	9.06	8.77
65	17 29 44.00	-18 32 58.0	wise(172944-183258)	A(l)	10.7	
66	17 26 41.91	-18 15 26.5	wise(172642-181526)	A	10.8	
67	17 31 35.00	-18 50 11.0	wise(173135-185011)	A(l)	11.2	
68	17 26 30.67	-18 37 31.5	SAO 160576	Ap	9.46	9.35
69	17 23 25.40	-17 58 15.7	SAO 160513	A2III/IV	8.81	8.59
70	17 11 29.57	-16 29 30.8	SAO 160347	A7V	7.78	7.52
71	17 25 20.62	-18 16 53.4	SAO 160533	A0V	8.73	8.58
72	17 32 21.00	-19 03 28.0	wise(173221-190328)	A(l)	10.7	
73	17 22 18.00	-17 53 15.0	wise(172218-175315)	A(l)	11.3	11.3
74	17 28 08.00	-18 36 23.0	wise(172808-183623)	A(l)	10.4	
75	17 19 53.35	-17 45 23.6	SAO 160462	A0V	6.06	6.04
76	17 33 15.10	-19 22 37.9	SAO 160630	B9IV	9.74	9.52
77	17 16 11.00	-17 19 47.0	wise(171611-171947)	A(e)	11.4	
78	17 21 15.86	-18 02 54.4	SAO 160487	B9.5V	9.45	9.40
79	17 24 37.04	-18 26 44.7	SAO 160523	B8V	6.38	6.21
80	17 22 50.51	-18 11 19.9	SAO 160506	A7III/IV	9.98	9.66
81	17 37 32.10	-20 03 15.4	SAO 185560	A0V	10.2	9.1
82	17 17 01.95	-17 39 25.1	SAO 160422	A0V	9.03	8.86
83	17 35 33.30	-19 53 48.2	HD 159432	A0V	9.1	8.1
84	17 23 24.00	-18 26 06.0	wise(172324-182606)	A(e)	11.3	
85	17 17 33.10	-17 52 13.7	SAO 160429	B9V	9.46	9.41
86	17 14 21.67	-17 27 57.9	SAO 160393	B9III/IV	8.20	8.15
87	17 12 15.33	-17 14 47.5	SAO 160354	AIV	7.62	7.57
88	17 27 02.69	-18 59 31.1	SAO 160551	B9Ib/II	9.84	9.48
89	17 38 33.00	-20 17 28.0	wise(173833-201728)	A(l)	10.4	
90	17 24 28.57	-18 50 49.8	SAO 160522	A0V	9.20	9.04
91	17 30 38.78	-19 33 27.0	SAO 160595	A2III	9.3	8.1
92	17 16 44.13	-17 55 41.6	wise(171644-175542)	A(e)	11.4	
93	17 27 51.28	-19 17 07.3	HD 158052	B9V	10.56	10.16
94	17 39 17.88	-20 42 32.4	SAO 185596	B9V	9.41	9.3
95	17 34 23.61	-20 06 11.3	SAO 185516	A0III/IV	10.24	10.04
96	17 15 31.00	-17 50 54.0	wise(171531-175054)	G	12.7	
97	17 19 43.00	-18 21 54.0	wise(171943-182154)	no sp	>15	
98	17 10 20.17	-17 19 44.6	HD 155108	A0III	9.96	9.77
99	17 12 28.74	-17 36 13.0	SAO 160359	A9V	8.69	8.35
100	17 25 47.96	-19 15 05.9	HD 157732	A0/A1V	10.16	9.83
101	17 37 50.53	-20 40 03.5	HD 159880	B8/B9V	9.60	9.48
102	17 16 06.00	-18 31 00.0	HD 156587	nebula		
103	17 35 46.09	-20 27 59.1	wise(173546-202759)	A(e)	10.8	
104	17 15 44.20	-18 10 54.0	HD 155992	A3II/III	9.4	9.3
105	17 20 15.74	-18 49 24.9	SAO 160469	B2II	9.40	9.29
106	17 26 23.96	-19 31 04.3	SAO 160542	A0 V	9.63	9.32
107	17 38 45.61	-20 57 37.6	SAO 185585	B8Ib/II	9.64	9.49
108	17 20 53.57	-18 54 12.1	HD 156895	B8III	10.45	10.37
109	17 22 30.14	-19 06 09.9	SAO 160501	B9.5V	9.76	9.54
110	17 35 21.46	-20 39 28.7	HD 159394	A0IV	10.42	10.3
111	17 14 27.65	-18 12 24.6	HD 155791	A0IV	10.8	10.6
112	17 09 04.51	-17 34 09.7	SAO 160315	A0V	8.43	8.33
113	17 34 13.00	-20 33 44.0	wise(173413-203344)	A	11.0	
114	17 13 54.58	-18 13 07.6	SAO 160385	A9V	8.56	8.3
115	17 36 46.25	-20 57 22.5	SAO 185548	A2V	8.46	8.06
116	17 35 39.35	-20 48 35.2	SAO 185535	A1III	9.14	8.88
117	17 15 29.18	-18 25 37.6	HD 155957	A2/3II	10.57	10.27
118	17 12 29.39	-18 08 12.8	SAO 160358	B8II	9.12	9.12
119	17 15 04.00	-18 26 00.0	wise(171504-182600)	A(e)	11.7	
120	17 23 16.16	-19 26 55.4	SAO 160511	A2III	8.43	8.04
121	17 40 14.70	-21 21 29.7	wise(174015-212130)	B	11.4	11.3
122	17 25 29.26	-19 44 27.1	SAO 160534	F0V	8.54	8.26
123	17 37 33.64	-21 10 22.3	wise(173734-211022)	A(e)	11.2	10.8

Id no.	α_{2000}	δ_{2000}	Proposed id.	Sp. Type	m_b	m_v
124	17 26 48.12	-19 59 15.8	HD 157898	A3II/III	10.2	9.1
125	17 11 06.26	-18 09 30.0	SAO 160341	A0IV/V	10.28	10.17
126	17 34 48.00	-21 03 00.0	HD 159290	B9V	11.8	10.8
127	17 27 13.90	-20 18 52.6	SAO 185414	B9III	9.34	9.19
128	17 24 39.00	-19 57 08.0	wise(172439-195708)	A(e)	11.3	
129	17 17 29.82	-19 09 10.7	HD 156289	B9.5II	11.1	10.9
130	17 12 40.45	-18 33 19.9	SAO 160363	A0II	9.46	9.17
131	17 11 57.65	-18 28 00.4	HD 155377	B9IV/V	11.0	10.7
132	17 37 19.99	-21 32 20.8	SAO 185555	B9IV	9.84	9.64
133	17 08 27.05	-18 10 12.3	SAO 160309	B9V	8.38	8.33
134	17 36 46.00	-21 32 35.0	wise(173646-213235)	A(e)	10.8	
135	17 36 16.78	-21 28 05.5	wise(173617-212806)	A(l)	11.4	11.2
136	17 27 14.70	-20 27 51.4	HD 157954	B9	10.7	10.7
137	17 09 07.52	-18 15 22.8	SAO 160317	A7III	8.79	8.49
138	17 29 02.74	-20 45 21.6	wise(172903-204522)	B(e)	11.4	10.9
139	17 19 56.31	-19 42 15.6	HD 156719	A3III	8.24	8.00
140	17 13 41.15	-18 58 39.0	SAO 160381	A9V	8.85	8.57
141	17 25 31.77	-20 19 10.2	SAO185386	A4II	9.91	9.56
142	17 22 34.20	-20 04 09.9	HD 157185	B9V	10.52	10.27
143	17 16 28.64	-19 20 14.3	HD 156095	A9V	8.97	8.53
144	17 08 19.08	-18 22 41.5	SAO 160307	A1IV	8.96	8.79
145	17 23 17.16	-20 13 49.4	HD 157312	B9III	10.34	10.16
146	17 36 00.00	-21 42 25.0	wise(173600-214225)	A(l)	10.6	
147	17 10 41.36	-18 45 17.7	SAO 160334	B9II/III	10.0	
148	17 20 51.00	-20 02 29.0	wise(172051-200229)	A(l),F	11.4	
149	17 14 44.00	-19 24 57.0	wise(171444-192457)	A	11.4	
150	17 32 50.64	-21 34 18.2	HD 158939	A0V	10.76	10.5
151	17 25 51.45	-20 46 48.3	SAO 185393	A0V	9.17	8.96
152	17 15 37.00	-19 33 00.0	wise(171537-193300)	G(e)	13.1	
153	17 37 26.91	-22 04 41.6	HD 159781	A0IV	10.36	10.1
154	17 35 18.50	-22 02 37.8	SAO 185526	Ap	6.49	6.57
155	17 18 31.60	-19 58 30.7	HD 156490	B9III	10.19	10.01
156	17 15 00.72	-19 32 31.8	SAO 160399	B9IV	9.70	9.51
157	17 25 25.89	-20 50 58.3	SAO 185384	B9III	9.70	9.60
158	17 31 03.46	-21 29 07.0	HD 158596	Ap	9.17	8.94
159	17 21 51.28	-20 25 03.4	HD 157055	A3II/III	10.45	10.29
160	17 33 09.82	-21 45 40.7	SAO 185498	A1/A2IV	9.88	9.62
161	17 20 55.47	-20 21 35.1	SAO 185294	A0V	10.02	9.89
162	17 21 06.87	-20 29 08.1	SAO 185302	A8/A9V	9.1	8.83
163	17 17 55.84	-20 10 28.1	wise(171756-201028)	A(e)	10.89	10.6
164	17 22 03.96	-20 44 29.0	SAO 185323	B9.5IV/V	9.36	9.04
165	17 36 29.03	-22 26 27.9	SAO 185545	B8IV	8.95	8.85
166	17 10 14.94	-19 26 10.6	SAO 160326	B8Ib/II	6.945	7.03
167	17 38 03.82	-22 34 54.9	SAO 185572	F5V	8.47	8.13
168	17 34 12.38	-22 13 20.5	SAO 185515	B8IV	9.53	9.43
169	17 21 33.00	-20 44 40.0	wise(172133-204440)	A(l)	11.5	
170	17 32 31.24	-22 02 32.4	HD 158858	A2III	10.58	10.25
171	17 24 09.00	-21 05 49.0	wise(172409-210549)	A(l)	10.9	
172	17 18 52.38	-20 29 57.4	SAO 185258	F0V	8.97	8.62
173	17 36 02.25	-22 32 33.6	SAO 185540	A0IV	8.69	8.51
174	17 31 35.30	-22 02 57.1	SAO 185473	B6II	10.56	10.14
175	17 17 53.78	-20 27 49.7	SAO 185236	B9III/IV	9.66	9.60
176	17 25 57.42	-21 24 58.7	SAO 185396	Ap	9.65	9.29
177	17 15 18.73	-20 17 41.2	SAO 185201+	A3V	9.44	9.14
	17 15 17.69	-20 16 24.0	HD 155927	A8V	9.77	9.36
178	17 22 25.08	-21 08 31.8	SAO 185332	B9IV/V	10.53	10.3
179	17 19 23.00	-20 46 172.0	wise(171923-204617)	F(e)	>13	
180	17 25 43.19	-21 37 40.1	HD 157706	B9III	10.87	10.8
181	17 21 00.37	-21 06 46.6	SAO 185296	F2/F3V	4.78	4.38
182	17 18 31.41	-20 48 19.6	SAO 185248	A2III	9.66	9.41
183	17 08 53.41	-19 40 35.1	SAO 160311	A0IV	9.80	9.69
184	17 33 33.09	-22 38 54.4	SAO 185504	A6IV	9.49	9.18
185	17 19 20.65	-21 04 29.4	HD 156601	B9.5IV	10.48	10.3
186	17 17 25.65	-20 55 39.9	SAO 185229	A3	10.19	9.92
187	17 22 04.00	-21 26 51.0	wise(172204-212651)	B(l)	10.0	

Id no.	α_{2000}	δ_{2000}	Proposed id.	Sp. Type	m_b	m_v
188	17 18 13.75	-21 00 32.8	wise(171814-210033)	A(e)	10.1	
189	17 20 42.74	-21 18 58.7	wise(172043-211859)	A(e)	10.1	
190	17 11 21.99	-20 25 29.0	SAO 185122	B9IV	7.50	7.52
191	17 33 45.31	-22 58 41.6	SAO 185509	A0V	9.87	9.61
192	17 17 02.00	-21 09 08.0	wise(171702-210908)	A(e)	10.3	
193	17 06 56.50	-19 56 45.8	SAO 160283	A0III	9.18	9.08
194	17 12 11.79	-20 37 18.7	wise(171212-203719)	A(e)	11.1	10.4
195	17 08 32.48	-20 13 03.1	SAO 185067	A0IV	7.94	7.79
196	17 34 07.54	-23 13 59.1	SAO 185513	A1IV	10.27	9.98
197	17 14 54.89	-21 06 00.3	HD 155847	B5III	10.12	9.94
198	17 09 44.32	-20 22 48.62	SAO 185090	A2II/III	10.27	10.05
199	17 18 38.77	-21 35 21.8	SAO 185252	B3III	9.88	9.52
200	17 30 34.34	-23 02 14.8	wise(173034-230213)	A(e)	9.4	
201	17 31 03.02	-23 10 30.8	SAO 185467	B7III	9.14	8.94
202	17 10 06.08	-20 47 01.2	HD 155064	B9V	9.57	9.37
203	17 22 54.62	-22 21 03.8	wise(172255-222103)	B(e)	11.4	11.1
204	17 28 45.00	-22 56 20.0	wise(172845-225620)	A(e)	11.0	
205	17 19 50.42	-21 57 00.6	wise(171950-215700)	A(e)	11.3	11.1
206	17 18 45.81	-21 53 11.0	HD 156503	A0III	10.83	10.5
207	17 23 52.66	-22 36 25.8	wise phot no cand	NO ID		
208	17 06 34.44	-20 42 41.3	HD 154498	B9III	10.42	10.31
209	17 22 37.71	-22 42 01.8	SAO 185333	A1III/IV	9.48	9.1
210	17 12 39.53	-21 36 21.8	SAO 185150	F2V	7.6	6.8
211	17 18 21.00	-22 15 20.0	wise(171821-221520)	B(e)	10.8	
212	17 23 13.10	-23 00 34.4	SAO 185349	B9V	7.46	7.40
213	17 30 58.02	-23 52 55.2	wise(173058-235255)	A	>14	
214	17 08 28.31	-21 20 13.4	HD 154804	A0IV	11.2	10.9
215	17 18 54.79	-22 42 28.2	SAO 185257	F0V	9.53	9.13
216	17 11 25.52	-21 53 50.6	SAO 185123	A5IV	9.46	9.05
217	17 10 43.91	-22 00 16.5	SAO 185109	A2/A3IV	9.25	8.94
218	17 18 27.28	-22 57 39.7	wise(171526-225432)	A(e)	10.72	10.28
219	17 24 24.51	-23 43 02.1	SAO 185361	B9III	10.34	10.00
220	17 15 12.80	-22 41 31.0	CPD-22 11931	B	9.8	
221	17 24 51.63	-23 55 33.9	SAO 185369	B5III	9.07	8.77
222	17 26 22.22	-24 10 31.1	SAO 185401	A3m	4.437	4.166
223	17 09 10.80	-22 15 29.0	wise(170911-221529)	A(l)	>14	
224	17 12 23.44	-22 55 30.8	SAO 185143	A5V	8.18	7.86
225	17 25 10.75	-24 36 18.7	SAO 185375	B9	8.63	8.39
226	17 18 59.09	-24 00 51.7	SAO 185259	A2III/IV	9.94	9.75
227	17 20 42.59	-24 16 16.7	SAO 185287	B3V	9.03	8.87
228	17 23 53.80	-24 51 25.5	wise(172354-245126)	A(l)	11.6	10.9

Table 3. Distribution of UV sources

m_{UV}	B0 – B9	A0 – A9	F0 – F9	G0 – G9	No sp
5–6	2	1	0	0	0
6–7	2	3	0	0	0
7–8	10	3	0	1	0
8–9	10	7	0	0	0
9–10	23	17	1	0	0
10–11	18	41	1	3	0
11–12	9	46	4	1	2
12–13	5	13	1	0	1
13–14	0	2	0	0	0
14–15	0	0	0	0	0
>15	0	1	0	0	0
Total	79	134	7	5	3

stars is negative, while normal G stars are much brighter in the visual range than in the UV. Such a strong UV excess may be due to the presence of some coronal activity or of a hot companion hidden by the late -type star.

Six UV sources are identified with Am or Ap stars. These stars are known to have weak UV flux with respect to

the regular A-type stars. While this is true for the Am stars identified with the UV sources N.64 and N.222, the [UV-v] colors of Ap stars cover the range of normal A-type stars.

Fig. 7 shows the distribution of the FAUST magnitude versus the instrumental (UV-v) color. There are two points at the extremes of Fig. 7.

The object at the extreme right, N.74, is the faintest UV source detected in this sample and the error in its UV flux is very large ($\simeq 45\%$); this affects the error in the color index as well. The point at the extreme left corresponds to source N.228. The (FAUST-v) color of this object is very negative, as expected for a very hot object or a subdwarf. Below we will show that this object is indeed a white dwarf.

5.1 A search for Hidden Subluminous Stars

No white dwarf (WD) or hot subdwarf (sd) stars were found as optical counterparts of the FAUST sources using the methods described above. This result is similar to that found in the identification of UV sources in the Virgo FAUST field

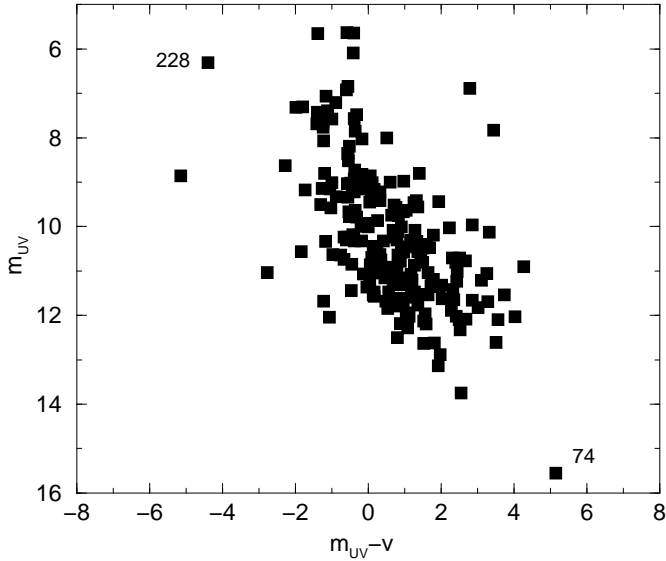


Figure 7. Distribution of the FAUST m_{UV} magnitude versus the color $m_{UV} - v$, for all the 227 identified sources.

(Brosch et al. 1997). A deficiency in hot evolved stars was found in other FAUST fields (e.g., Daniels et al. 2001). This could be the result of the lack of such objects in the catalogues from which possible counterparts are selected.

Hot subluminous stars are numerous among blue objects. Systematic colorimetric surveys, such as the Palomar Green (PG: Green et al. 1986) or the US Survey (Usher and Mitchell 1990), show that these objects indeed dominate the population of blue stars down to $B=16.5$.

Furthermore, far-ultraviolet surveys such as those by the ROSAT Wide Field Camera (Pye et al. 1995) and by the Extreme Ultraviolet Explorer (EUVE) (Bowyer et al. 1994, 1996) discovered a substantial number (120) of hot WDs (Barstow et al. 1994a, Barstow et al. 1994b, Marsh et al. 1997, Burleigh et al. 1997). The WDs detected by EUVE are very hot objects, with temperatures greater than several 10^4 K, whereas FAUST essentially covers lower effective temperatures. At the limit magnitude of our sample of $m_v \simeq 12$, a WD would be a very luminous object ($M_V \sim 10$). Very few such objects were found by the PG survey.

The number density of WD up to $M_V \sim 10$ in the PG survey is about 0.04 per 1000 pc^{-3} (Boyle 1989). With a maximal distance to detect WD with FAUST set at 25 pc, our sampled volume is $\simeq 150 pc^3$ with an expected total number of WDs to $M_V \sim 10$ of 6×10^{-3} . Furthermore, this prediction is an upper limit, since our sample of UV sources is not magnitude-limited.

In order to search for the missing sd/WD stars in our field we take advantage of the photometric and astrometric information provided by the Hipparcos satellite. We cross-identified our UV sources positions with objects in the Main Part of the Tycho catalog (ESA 1997). For all the UV stars under considerations a Tycho entry is available and a parallax value is significant for 46 entries. Table 4 gives the information retrieved from the Tycho catalog for all the stars and the derived distance (d) and absolute magnitude (M_V). Table 4 lists also the proper motion components in milliarc-sec/yr.

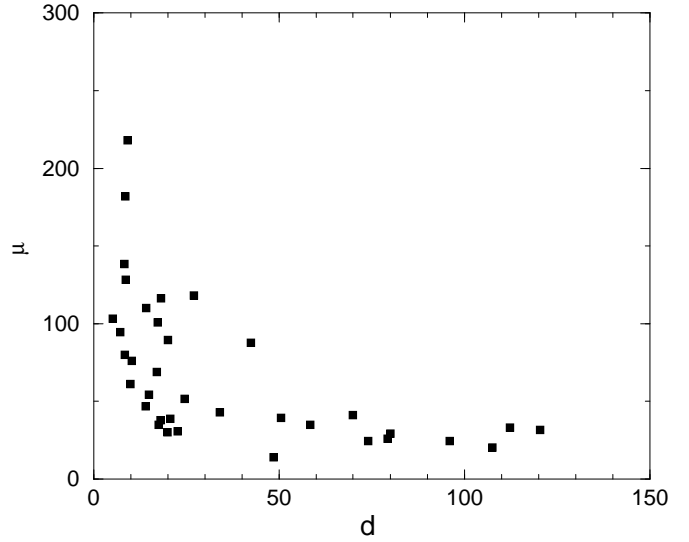


Figure 8. Distribution of the proper motion modulus μ (mas) with respect to the distance d (pc) for the sample of stars retrieved from the Tycho catalog.

Fig. 8 shows the distribution of the proper motion modulus (μ) with respect to the calculated distance (d). As expected for the low galactic latitude of the Ophiuchus field, the sample is composed of stars with small proper motions, consistent with their membership in the disk.

The parallax precision (σ/π) is very large for all the stars in Table 4 but one, namely SAO 1854091 identified with the source N.222. The median errors of the Hipparcos and Tycho parallaxes increase with apparent magnitude. However, even at the faintest Hipparcos magnitudes ($V \geq 10.5$), the median error amounts to few milliarcsec(mas) (see The Hipparcos and Tycho catalogues, Fig 3.2.26 and Fig. 3.2.39).

For Tycho parallaxes the median standard error is larger (see The Hipparcos and Tycho catalogues, Fig 3.3.14 and Fig. 3.3.16). For instance at Tycho magnitudes $V_T = 11$ it amounts to ~ 50 mas. The better precision for Hipparcos stars is implied by the different characteristic of the catalogues, where Hipparcos selected the brighter stars while the Tycho Catalog is a survey of all stars down to its sensitivity limits.

We neglected the presence of extinction in the line of sight and this omission impacts on the assigned absolute magnitude in Table 4. The interstellar extinction is very patchy (Schlegel et al. 1998) and in the Ophiuchus region A_v spans from 1 to more than 3 mag.

The parallax errors for almost all the entries in Table 4 are very large. Observation errors that exceed a few mas are an indication of systematic problems in the Hipparcos data reduction. A large error can indicate that the parallax is actually too small to be measured, or can be due to the presence of an undetected multiple system (Perryman et al. 1995)

Fig. 9 shows the histogram of the absolute magnitudes listed in Table 4. The spectral classification of these stars spans types from B to early F, and one would expect that M_V should be ≤ 3.9 (Allen 1973) if these would be main-

Table 4. Hipparcos data

Id no.	π (mas) $\pm\sigma$	d(pc)	M_V	Sp type	μ_α (mas/yr)	μ_δ (mas/yr)
16	10.4 \pm 6.4	96.1	2.92	A3III	21.5 \pm 8.1	-11.6 \pm 5.8
18	8.3 \pm 5.9	120.4	2.96	F2V	-27.2 \pm 5.8	-15.8 \pm 3.4
20	148.5 \pm 47.0	6.7	12.09	A		
24	29.3 \pm 22.8	34.1	7.66	A0III	-39.9 \pm 18.6	15.4 \pm 15.7
25	56.9 \pm 29.4	17.5	9.45	B9III	10.2 \pm 34.1	33.2 \pm 20.0
32	9.3 \pm 4.5	107.5	2.44	F0IV	-19.0 \pm 5.3	-6.8 \pm 2.6
37	13.5 \pm 8.8	74.0	4.45	B9IV	21.5 \pm 11.6	-11.7 \pm 8.0
43	54.8 \pm 35.0	18.2	9.19	B9IV	-66.3 \pm 32.8	-95.6 \pm 27.4
58	65.8 \pm 30.3	15.1	9.85	B9III		
62	96.3 \pm 59.1	10.3	10.95	A(e)	-5.0 \pm 46.1	-76.0 \pm 27.2
65	118.8 \pm 43.1	8.4	11.74	A(l)	77.8 \pm 35.6	-17.6 \pm 22.1
66	90.9 \pm 33.1	11.0	10.74	A(e)		
68	15.7 \pm 15.6	63.6	5.47	Ap		
70	8.7 \pm 5.4	114.9	2.55	A7V		
74	117.4 \pm 47.5	8.5	11.48	A(e)	157.1 \pm 49.2	91.8 \pm 28.6
76	21.2 \pm 15.3	47.1	6.43	B8IV		
80	48.3 \pm 18.9	20.7	8.49	A7III/IV	-34.5 \pm 18.6	-17.6 \pm 12.3
83	20.6 \pm 19.4	48.5	5.83	AV	6.5 \pm 13.8	-12.3 \pm 9.4
92	57.7 \pm 51.3	17.3	10.35	A(e)	-100.3 \pm 64.3	9.1 \pm 43.8
108	17.1 \pm 15.0	58.4	5.99	B9V	28.5 \pm 16.4	-20.3 \pm 12.0
111	67.1 \pm 43.4	14.9	10.06	A0IV	-53.2 \pm 46.7	-10.0 \pm 38.9
113	71.3 \pm 36.0	14.0	11.63	A(l)	20.9 \pm 34.7	-42.0 \pm 21.4
123	189.7 \pm 43.4	5.2	12.64	A(e)	5.1 \pm 54.9	-103.0 \pm 44.6
126	55.4 \pm 27.5	18.0	10.07	B9V	30.7 \pm 29.8	-22.2 \pm 20.4
127	12.6 \pm 11.4	79.3	4.88	A0IV	-21.8 \pm 12.2	-14.1 \pm 9.6
139	14.3 \pm 6.8	69.9	4.09	A3III	8.8 \pm 8.8	-40.1 \pm 5.4
148	108.3 \pm 61.3	9.2	11.85	A(l), F	217.1 \pm 49.5	21.3 \pm 42.7
150	100.3 \pm 27.9	9.9	10.83	A0V	13.7 \pm 28.1	-59.6 \pm 21.2
177	44.0 \pm 15.3	22.7	7.73	A3V	30.1 \pm 15.1	-6.0 \pm 9.7
	23.5 \pm 18.5	42.5	6.72	A8V	79.0 \pm 18.9	-38.1 \pm 11.2
178	50.2 \pm 24.6	19.9	9.09	B9IV	-9.2 \pm 31.1	-28.8 \pm 23.7
180	19.8 \pm 11.5	50.5	7.38	B9III	-24.4 \pm 13.0	-30.9 \pm 8.8
182	40.8 \pm 20.8	24.5	7.79	A2III	-23.8 \pm 17.4	45.9 \pm 14.3
191	36.1 \pm 20.3	27.7	7.73	A0V		
194	49.9 \pm 45.4	20.0	9.83	A(e)	-88.4 \pm 46.1	14.4 \pm 35.0
198	58.8 \pm 20.1	17.0	9.18	A2II/III	-67.9 \pm 22.7	-11.0 \pm 18.0
202	23.9 \pm 16.0	41.8	6.52	B9V		
205	53.5 \pm 49.2	18.6	10.03	A(e)		
206	114.0 \pm 38.2	8.7	11.19	A0III	-123.2 \pm 47.2	-35.7 \pm 26.2
210	8.9 \pm 4.3	112.3	2.22	F2V	32.9 \pm 5.4	-2.7 \pm 3.3
211	70.0 \pm 47.3	14.2	10.60	B(e)	25.0 \pm 56.9	-107.1 \pm 36.6
213	12.5 \pm 5.9	80.0	>9.5	A(l)	-27.6 \pm 5.3	-9.7 \pm 2.9
214	224.4 \pm 90.3	4.4	13.05	A0IV		
220	120.0 \pm 57.2	8.3	12.13	B	-92.4 \pm 53.00	102.90 \pm 41.50
222	36.8 \pm 2.9	27.1	2.34	A3m	-0.5 \pm 3.2	-118.2 \pm 2.0
228	139.1 \pm 71.8	7.18	12.44	A(l)	80.3 \pm 59.80	-49.90 \pm 34.60

sequence stars, while a significant number of objects in Fig. 9 have faint M_V values, as expected for WD or subdwarf stars. Note that the absolute V magnitude of a sdB subdwarf is $M_V = 4.2 \pm 0.7$ (Heber 1986), while that of WDs ranges from 9.5 to 16.5. Vauclair et al. (1997) analyzed the parallaxes obtained by the Hipparcos mission with values obtained through ground observations, including the one-sigma measurements, and found a 2/3 fraction of agreements, compatible with the listed 1 sigma errors. Reid (1997) and Gratton et al (1997) compared the parallax measurements from ground-based data with new ones obtained by the Hipparcos satellite for a sample of subdwarfs. The Hipparcos parallaxes are systematically smaller so that the derived absolute magnitude are on average brighter. After applying the statistical correction for the Lutz-Kelker systematic bias towards over-

estimating parallax measurements, the mean difference in absolute magnitude is 0.53 ± 0.14 mag.

The M_V calculated in Tab 4 for the stars of known spectral type seems systematically underestimated with the respect to the value corresponding to their spectral type and this effect is due to the inaccuracy of the parallax. The astrophysical interest of Tycho parallaxes is restricted to the brighter stars (Høg et al. 1997) Hence, we may conclude that the search for subluminescent stars on the basis of the parallax data of Table 4 is rather unreliable.

Many of the stars in Table 4 are catalogued as stars of known spectral type and some are stars observed at the Wise telescope during the identification program. It is possible, however, that some have not been recognized as subluminescent stars at the low resolution and low signal-to-noise quality of

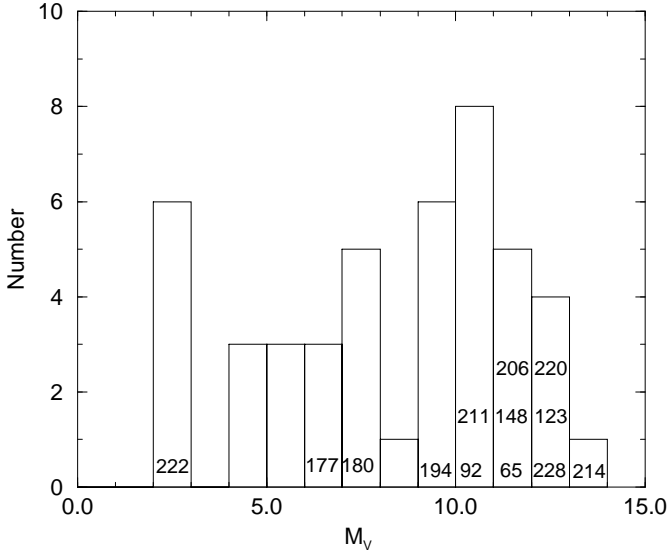


Figure 9. Histogram of the absolute magnitude for the UV sources listed in the Tycho catalog.

the spectra obtained for the FAUST sources identification program.

In an effort to find the most probable subluminous stars among the FAUST stars, we calculated the predicted UV flux at the FAUST wavelength, performing synthetic photometry (section 5.2). Furthermore, we embarked in a follow-up spectroscopic observational program of the candidates, i.e., of the objects showing a FAUST magnitude much brighter than the predicted one (section 5.3). The purpose of these observations was to cull the high gravity stars from the sample of ultraviolet-excess objects, by checking the Balmer line profiles against models.

5.2 Predicting the expected UV magnitude

In order to find the most probable subluminous stars hidden among dwarf stars, we calculate the predicted UV flux of a star of a given spectral type and luminosity, using synthetic photometry from spectral data. A code has been developed (Formigini, in preparation) that uses theoretical and empirical stellar libraries (mainly from IUE). For each specific wavelength and specific filter, the code is able to predict the monochromatic magnitude

$$UV_{\lambda} = -2.5 \log f_{\lambda} + const \quad (2)$$

If no spectral information is available for a star, the (B-V) color is used and the UV magnitude is predicted only on the basis of the photometric information. This code has already been successfully tested for the Virgo FAUST sources listed in the Tycho catalog. The magnitudes predicted for the Virgo UV sources are well-correlated with the FAUST measured ones. A complete discussion of the results of this code, applied to all the FAUST sources, will be presented in a forthcoming paper (Formigini, in preparation). A preliminary version of this code has been tested on the photometric data set of the TD-1 catalog (Thompson et al. 1978) with satisfactory results.

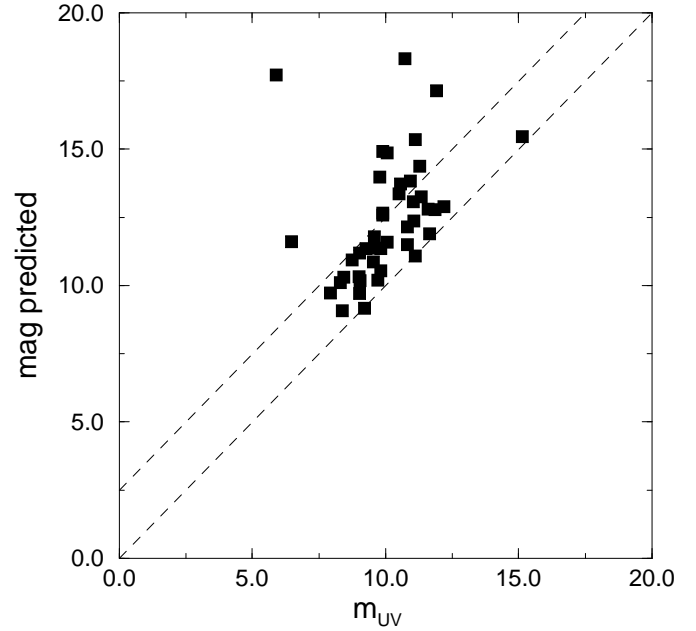


Figure 10. FAUST magnitudes with respect to the predicted ones.

We applied the code to the sample of 46 stars identified as counterparts of the Ophiuchus FAUST sources for which parallaxes are listed in the Tycho catalog. The visual and blue magnitudes listed in the Tycho catalog have been used for the prediction of the UV magnitudes. The magnitude calculated by the code can be used as an indication of the UV emission expected if the object is a main-sequence star. Fig. 10 shows the measured FAUST magnitudes with respect to the predicted ones. The predicted magnitudes are fainter than the measured ones by one to two magnitudes; this systematic effect will be addressed in the forthcoming paper.

However, the relevant result of the prediction for the present discussion is the definition of a region inside the dotted lines in Fig. 10, which is populated by the majority of the stars listed in Table 4. There are 13 stars outside this region for which FAUST measured a brighter UV magnitude than the one predicted on the basis of the photometric color.

In Fig. 9 we marked, in each magnitude bin, the number of the UV source as listed in Table 1 of each such star. According to their M_V , all these stars but one, should belong to the subdwarf or white dwarf luminosity classes. The source N. 222 is classified as an Am star and the metallic lines affect the (B-V) color used for the prediction. Actually, there are twelve ultraviolet excess sources with $M_V \geq 5$; these are the best candidates for hidden subluminous stars.

5.3 Spectroscopic Observations

The twelve UV sources with $M_V \geq 5$ and with a predicted FAUST magnitude much brighter than the measured one, as explained in the previous paragraph, were observed with

the 1.0 meter telescope at the Wise Observatory. The FOSC was used with a 2" slit and a 600 g/mm grism. This yields a wavelength coverage from $\sim 3400\text{\AA}$ to $\sim 7100\text{\AA}$ at a spectral resolution of $\sim 3.67\text{\AA}$ per pixel. Although the spectral resolution is not significantly higher than that used in the earlier identification observations, the exposure times were longer in order to achieve a good signal-to-noise.

The spectra were reduced using standard techniques. Pixel-to-pixel sensitivity variations were removed using flat-field spectra acquired at the beginning of each night, and wavelength calibration was achieved using He-Ar arc spectra observed after each object spectrum. A bright star of known spectroscopical type was observed with the same configuration as used for program stars. The spectra could not be flux calibrated, owing to the narrow slit compared to the seeing size; some of the starlight was lost. Since the purpose of these observations is to cull high-gravity stars from the sample, only relative calibration in a restricted spectral segment is required for profile analysis.

5.4 The line profiles

Table 5 lists the observed objects. The spectra of source N.92 were of bad quality and were discarded. A visual inspection of the higher quality spectra reveals the presence of moderately broadened Balmer lines for all the objects observed but one, N. 220. Broad and shallow Balmer lines are the characteristic allowing us to isolate the subdwarf class among the hot stars, since line profiles depend very sensitively on the value of gravity (g) and on temperature (T_{eff}). The absence of the absorption line He II 4686 indicates that the sdO class cannot be assigned to one of the nine objects discussed here.

A reliable determination of stellar atmospheric parameters can be obtained by simultaneously fitting observed line profiles to appropriate model atmospheres. This has been done by many authors using grids of model stellar atmospheres. For instance, such models, in local thermodynamic equilibrium (LTE) and non-LTE, and taking into account the blanketing process, have been computed and used by Saffer et al. (1994) for sdB stars. However the models used by Saffer et al. have not been published.

We found in the literature available models which are the results of a grid of LTE and of some NLTE and blanketed pure-hydrogen models, calculated by Wesemael et al. (1980). These pioneering models are still valid for the aim of our analysis. The influence of NLTE effects and metal-line blanketing on hydrogen line profiles of high gravity stars has been investigated by Napiwotzki (1997) and by Barstow et al. (1998). The NLTE effects are significant only at highest temperatures and at low $\log g$, and the differences are detected only in the core and only at high spectral resolution (Saffer 1994). The metal-line blanketing is more dominant at the the temperature of sdB (see Napiwotzki (1997), fig 10) and should be taken into account for an accurate determination of the atmosphere parameters. More recently, a completely new grid of stellar atmosphere models have been calculated (Barstow et al 2001) using the code TLUSTY (Hubeny and Lanz 1995).

Since the aim of this work is to isolate the subluminescent stars, without embarking in an accurate determination of the atmospheric parameters, we compared the Balmer profiles

of the observed spectra with the LTE unblanketed model profiles published by Wesemael et al. (1980).

The theoretical line profiles were convolved with the instrumental resolution profile. This profile was determined from the emission lines produced by the He-Ar comparison lamp, and was approximated by a Gaussian profile of FWHM $\sim 6.2\text{\AA}$. No simulated continuum, such as a Poisson noise, was added to the model profiles, and no convolution with a rotation broadening function was performed. Rotation could affect the line cores, while we are interested in the change in the line wings due to effective temperature and surface gravity variations. Saffer et al (1994) found that only for very large velocities ($\geq 100 \text{ km s}^{-1}$) the stellar rotation can perturb the line wings.

Around the Balmer line rest wavelength, two symmetrical 100\AA segments of the observed spectrum were extracted, sufficiently far from the line to define adequately the continuum on either side of it. The local slope of the continuum was subtracted from the spectrum. The observed and theoretical line profiles were interpolated and rectified to a linear continuum in a consistent manner.

Fig 11 shows the $H\beta$ line profile for the nine objects observed. In some profiles there is a residual systematic deviation in the continuum spectral slope between the model and the data, which should be dealt with for an accurate analysis. The dashed line in Fig 11 is the model profile from Wesemael et al. (1980) for $\log g=6$ and $T_{eff} = 30000\text{K}$. For N.214 and N.228 the dashed line corresponds to a higher gravity model, while the source N.220 shows a narrow line profile.

A proper model atmosphere analysis requires a simultaneous line-by-line analysis. The models in Fig 11 are only indicative and we do not claim that this fitting is a final and authoritative determination of the exact temperature or/and gravity. We can only state that low-gravity models, such as for dwarf stars, are inappropriate for all the candidates observed but N.220.

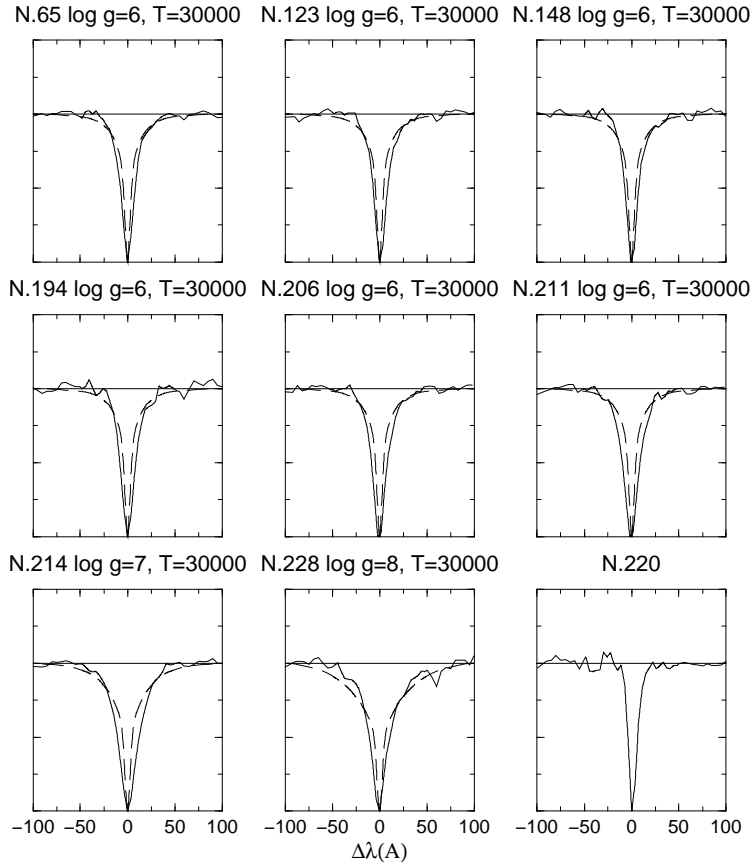
Another approach is to compare the spectral profile with real stellar atmospheres, such as the spectrum of a dwarf star and of a white dwarf observed under the same conditions as the candidate stars. We observed WD 2032+248 (G186-31), classified as a DA white dwarf with atmospheric parameters $T_{eff} = 19980\text{K}$ and $\log g=7.83$ (Bergeron et al. 1992), and the A0 V star BD +26 2606, which was observed every night. Fig 12a and Fig 12b show the $H\beta$ line profile of BD +26 2606 superposed to that for the objects N.211 and N.228. In Fig 12c the $H\beta$ line profile for WD 2032+248 is compared with that of N.228. These comparisons enhance the reliability of the classification of the candidates as sdB/WD stars.

Our spectral data are a fair confirmation of the presence of high-gravity atmospheres, i.e., of the presence of a substantial number of subluminescent stars in the Ophiuchus FAUST sample. Two of the observed candidates can be fitted with atmospheres of $\log g \geq 7$, as for white dwarfs stars, and six are sdB stars.

Many sdB stars are members of binary systems with cool companions. Analyzing the spectral distribution of a sample of 34 sdB, Aznar Cuadrado and Jeffrey (2001) estimate the sdB binary fraction between 56 % to 100% that have a main sequence star companion. The presence of an

Table 5. Candidates subluminous stars

Id no.	listed Sp. Type	m_v	π (mas) $\pm\sigma$	UV-excess mag	New classification
65	A(l)	10.7	118.8 ± 43.2	5.0	sdB
92	A(e)	11.4	57.7 ± 51.3	4.2	not observed
123	A(e)	10.8	189.7 ± 43.4	4.2	sdB
148	A(l),F	11.4	108.3 ± 61.3	2.9	sdB
177	A8V	9.8	23.5 ± 18.5	2.7	not observed
180	B9III	10.9	19.8 ± 11.5	4.8	not observed
194	A(e)	10.4	49.9 ± 45.4	7.6	sdB
206	A0III	10.5	$114. \pm 38.2$	2.9	sdB
211	B(e)	11.	70.0 ± 47.3	3.1	sdB
214	A0IV	10.9	224.4 ± 90.3	3.2	wd
220	B	10	$120. \pm 57.2$	5.2	B
228	A(l)	10.9	139.1 ± 71.8	11.8	wd


Figure 11. The $H\beta$ profile observed (line) and the model atmospheres profile (dashed) at the marked temperature and gravity, for the nine candidates.

undetectable binary companion could indeed be the source of the inaccuracy of the astrometric data.

The spatial distribution of sdB is important for a description of their evolutionary scenario and for the links with other types of stars. sdB stars are one of the evolutionary channels and direct progenitors to white dwarfs. The space density of sdB at bright magnitudes is poorly defined. Complete samples are needed for such investigations, or alternatively a reliable estimate of the completeness of such samples. However the uncertainty on the scale-height distri-

bution adopted, uniform or exponential, make the completeness correction quite difficult.

The PG survey is one of the largest and most studied survey of sdBs. It is, however, generally accepted that the PG sample is quite incomplete at bright magnitudes ($\leq B=12.5$). Villeneuve et al (1995) review the problem of completeness and give a revised space density of $3 \pm 1 * 10^{-7} \text{ pc}^{-3}$ and an exponential scale height of the order of $450 \pm 150 \text{ pc}$, or alternatively an isothermal disk scale height of $600 \pm 150 \text{ pc}$. Mitchell (1998) claims a mix of disk and halo populations. A significant halo component for sdB stars sup-

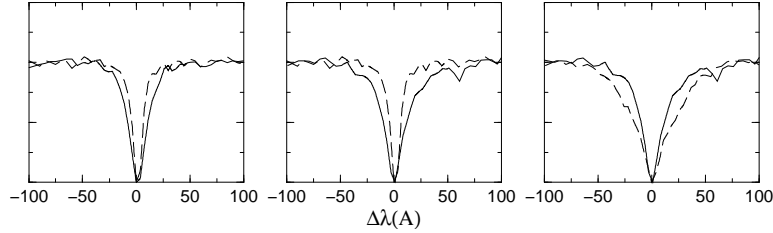


Figure 12. The $H\beta$ profile of BD+26 2606 (dashed) compared a) with that for N.211 (line) and b) with that for N.228 (line); c) The $H\beta$ profile for WD 2032+248 compared with that for N.228 (line).

ports the hypothesis of similar spatial distributions for sdB and sdO stars and hence the possibility of an evolutionary process relating sdB and sdO.

A comprehensive search for previously unrecognized subdwarfs in the Hipparcos catalogue has been carried out by Reid et al (2001). Among the stars with parallaxes measured to a precision better than 15 per cent, only few (nine) such stars were discovered. Our analysis shows that combining the UV information with even poorly determined parallaxes, some new sdB are detected, and that indeed more such bright stars are still unrecognized in the existing samples. We are extending this analysis to the other FAUST fields previously identified at the Wise Observatory.

5.5 Possible members of the Ophiuchus molecular cloud

The Hipparcos distance of four stars in Table 4 is comparable to the distance of the Ophiuchus molecular cloud with which they appear associated, and their position is about 12° away from the ρ Ophiuchus core. Their mean transverse velocity, calculated from the proper motion, is 14 km s^{-1} .

Star formation in molecular clouds occurs in two different environments; in small, isolated and dense regions distributed throughout the molecular cloud, such as in Orion, or in a single massive concentration of dense gas, such as the ρ Ophiuchi core (Lada et al. 1993). The accumulation of dense gas evolves through star formation, to form an embedded cluster of stars. Dynamical relaxation process, such as energy equipartition, leads to the massive stars releasing potential energy and sinking towards the center while the less massive stars gain kinetic energy and "evaporate" leaving the cluster and the cloud.

The four stars which have the distance of the Ophiuchus cloud have spectral type later than A7 and are not massive. We suggest that these four stars could have escaped the young cluster by this process of stellar-dynamical evaporation and migrated far away from the region of their formation. At a distance of 125 pc, and with a mean velocity of 14 km s^{-1} , the evaporation process took place some 3 Myr ago.

6 CONCLUSIONS

We have analyzed the UV FAUST image in the direction of the Ophiuchus molecular cloud and detected 228 UV sources. Optical identification was presented for all sources.

Multicolor broad-band photometry was used in selecting the candidates, followed by low-resolution spectroscopy. Spectral types are presented for 60 stars newly identified as optical counterparts of the UV sources. Most of the UV sources were identified as early-type stars. The Hipparcos/Tycho information was used to calculate the absolute magnitude of these stars. Some 39 UV sources are associated with hot sub-luminous stars, however, the large errors in the parallax measurements prevent a conclusive classification of them as sd/WD stars.

Synthetic photometry of spectral data was performed in order to predict the expected UV emission, on the basis of the photometric information from Tycho. The comparison of the predicted emission with the FAUST measured magnitudes allowed us to select twelve stars as highly probable hot stars. High signal-to-noise spectra were obtained for nine of these stars and Balmer line profiles were compared with the prediction of atmosphere models and with the spectrum of real stellar atmospheres. Among the nine candidates, six were classified as previously unrecognized sdB stars and two as white dwarfs. The lack of completeness of our sample prevented us from estimating of the local density of subdwarfs. However, our result indicates that more bright subluminescent stars are missed in the existing samples.

ACKNOWLEDGMENTS

The UV astronomy effort at Tel Aviv is supported by special grants to develop a space UV astronomy experiment (TAU-VEX) from the Ministry of Science, and from the Austrian Friends of Tel Aviv University. Part of this study was supported by a grant from the US-Israel Bi-national Science Foundation. Observations at the Wise Observatory are supported by a Center for Excellence Grant from the Israel Science Foundation. This paper made use of the SIMBAD data base operated at CDS, Strasbourg, France. We acknowledge help with this project, at various stages, from Ms. Susanna Steindling, Ms. Orly Kovo and Mr. E. Goldberg and discussions with Martin Barstow.

REFERENCES

- Allen C.W., 1973, *Astrophysical Quantities*, London: The Athlone Press, Univ. of London.
- Aznar Cuadrado, R. and Jeffrey, C.S. 2001, *A&A*, 371, 638
- Barstow M.A., Holberg J.B., Fleming T.A., Marsh M.C., Koester D. and Wonnacott D., 1994a, *MNRAS*, 270, 499

- Barstow M.A., Holberg, J.B., Marsh M.C., Tweedy R.W., Burleigh M.R., Fleming T.A., Koester D., Penny A.J. and Sansom A.E., 1994b, MNRAS, 271, 175
- Barstow M.A., Hubeny I. and Holberg J.B., 1998, MNRAS, 299, 520
- Barstow M.A., Holberg J.B., Hubeny I., Good S.A., Levan A.J. and Meru F., 2001, MNRAS, 328, 211
- Bergeron P., Saffer A.R. and Liebert J., 1992, ApJ, 394, 228
- Boyle B., 1989, MNRAS, 240, 533
- Bowyer S., Sasseen T.P., Lampton M. and Wu X., 1993, ApJ, 415, 875
- Bowyer S., Lieu R., Lampton M., Lewis J., Wu X., Drake J.J. and Malina R.F., 1994, ApJS, 93, 569
- Bowyer S., Sasseen P.T., Xiauyi W. and Lampton M., 1995, ApJS, 96, 461 (FSC)
- Bowyer S., Lampton M., Lewis J., Wu X., Jelinsky P. and Malina R.F., 1996, ApJS, 102, 129
- Brosch N., Almozino E., Leibowitz E.M., Netzer H., Sasseen T., Bowyer S., Lampton M. and Wu X., 1995, ApJ, 450, 137
- Brosch N., Formiggin L., Almozino E., Sasseen T., Lampton M. and Bowyer S., 1997, ApJS, 111, 143
- Brosch N., Ofek E., Almozino E., Sasseen T., Lampton M. and Bowyer S., 1998, MNRAS, 295, 959
- Brosch N., Brook A., Wisotzki L., Almozino E., Prialnik D., Bowyer S. and Lampton M., 2000a, MNRAS, 313, 641
- Brosch N., Almozino E., Engels D., Bowyer S. and Lampton M., 2000b, MNRAS, 316, 58
- Burleigh M.R., Barstow M.A. and Fleming T.A. 1997, MNRAS, 287, 381
- Daniels J., Brosch N., Almozino E., Shemmer O., Bowyer S. and Lampton M., 2001, MNRAS, 324, 580
- ESA, 1997, The Hipparcos and Tycho Catalogues , ESA SP-1200
- Gratton R.G., Fusi Pecci F., Carretta E., Clementini G., Corsi C.E. and Lattanzi M.G. 1997, ApJ, 491, 749
- Green R.F., Schmidt M. and Liebert J., 1986, ApJS, 61, 305 (PG)
- Heber U., 1986, A&A, 155, 33
- Høg E. et al. 1997, A&A, 323, L57
- Hubeny I. and Lanz T. 1995, ApJ, 438, 875
- Jacoby G.H., Hunter D.A. and Christian C.A., 1984, ApJS, 56, 257
- Johnson H., 1966, ARA&A, 4, 193
- Lada, E.A., Strom, K.M. and Myers, P.C. 1993, in Levy E.H., Lunine J.I. and Matthews M.S. eds, Protostars and Planets III. University of Arizona Press
- Lampton M., Sasseen T.P., Wu X. and Bowyer S., 1993, Geophys. Res. Lett., 20, 539
- Lasker B.M., Jenkner H. and Russell J.L., 1997, Space Telescope Science Institute
- Marsh M.C., Barstow M.A., Buckley D.A., Burleigh M.R., Holberg J.B., Koester D., O'Donogue D., Penny A.J. and Sansom A.E., 1997, MNRAS, 286, 369.
- Mitchell, K.J., 1998, ApJ, 494, 256
- Napiwotzki R., 1997, A&A, 322, 256
- Perryman M.A.C. et al. 1995, A&A, 304, 69
- Pye J.P., McGale P.A., Allan D.J., Barber, C.R., Bertram D., Denby M., Page C.G., Ricketts M.J., Stewart B.C. and West R.G., 1995, MNRAS, 274, 1165
- Reid I.N., 1997, AJ, 114, 161
- Reid I.N., van Wyk F., Marang F., Roberts G., Kilkenny D. and Mahoney S., 2001, MNRAS, 325, 931
- Saffer A.R., Bergeron P., Koester D. and Liebert J., 1994, ApJ, 432, 351
- SAO 1966, Smithsonian Astrophysical Observatory Star Catalog, Washington: Smithsonian Institution, publication No. 4652
- Savage B.D. and Mathis J.S., 1979, ARA&A, 17, 73
- Schlegel D.J., Finkbeiner D.P. and Davis M., 1998, ApJ, 500, 525
- Silva D.R. and Cornell M.E., 1992, ApJS, 81, 865
- Thompson G.I., Nandy K., Jamar C., Monfils A., Houziaux L., Carnochan D.J. and Wilson R., 1978, Catalog of Stellar Ultraviolet Fluxes, The Science Research Council (TD-1)
- Turon C. et. al, 1993, Bull. Inf. CDS, 43 (Version 2 of the Hipparcos Input Catalog).
- Usher P.D. and Mitchell K.J., 1990, ApJS, 74, 885
- Vauclair G., Schmidt H., Koester D. and Allard N., 1997, A&A, 325, 1055
- Villeneuve B., Wesemael F., Fontaine G. and Carignan C. 1995, ApJ, 446, 646
- Wesemael F., Auer L.H., Van Horn H.M. and Savedoff M.P., 1980, ApJS, 43, 159